# Beam Spin Asymmetries from Exclusive $\pi^+ N$ Electroproduction

David M. Riser, Kyungseon Joo, Harut Avakian

January 2018

## Contents

# 1 Introduction

For more than 50 years QCD has been under experimental investigation. The simple fact that bound states of colored quarks and gluons have to have no net color (and therefore can't be observed as free particles) has pushed physicists to find ways to interrogate and study these fundemental degrees of freedom in QCD. The most abundant and stable bound states (here on earth) of QCD are protons and neutrons, and have been the laboratory for study of quarks and gluons.

The first studies to probe quarks and gluons within nucleons were performed at SLAC, when electron scattering was used to produce QED interactions between the charged electrons and the charged quarks. The experiments measured electron scattering cross sections in terms of a variable $x$ known as the momentum fraction. The momentum fraction is simply the fraction of the total nucleon momentum carried by the struck quark in the scattering event. Results of these experiments remain some of the strongest evidence for the belief that QCD is the correct theory of the strong interaction. More recently, theoretical advancements have led to formulations of inclusive and exclusive reaction cross sections in terms of new parametrizations that describe not only the longitudinal momentum fraction, but also the momentum space and spatial distribution of quarks in the plane transverse to the hard momentum transfer (the same direction in which x is measured).

## 1.1 Formalism

In this note, the exclusive reaction $ep \rightarrow e'\pi^+N$ is considered. The cross section for this process can be written down in a model independent way by using Lorentz invariance and conservation laws [1]. The structure functions can then be calculated by modeling quark-gluon dynamics using different formulations. In electron scattering experiments it is customary to define the momentum transfer $q$ (where $q = l - l'$ and $Q^2 = -q^2$).

$$\begin{aligned}\frac{d^4\sigma}{dE'd\Omega d\phi_h dt} = \Gamma\Big[&\sigma_T + \varepsilon_L\sigma_L + \sqrt{2\varepsilon_L(1+\varepsilon)}\sigma_{LT}\cos\phi_h + \\ &\varepsilon\sigma_{TT}\cos(2\phi_h) + \lambda\sqrt{2\varepsilon_L(1-\varepsilon)}\sigma_{LT'}\sin\phi_h\Big]\end{aligned} \tag{1}$$

Where the photon flux $\Gamma$ is given by,

$$\Gamma = \frac{\alpha_{em}}{2\pi^2}\frac{E'_e}{E_e}\frac{W^2 - m_p^2}{2m_pQ^2}\frac{1}{1-\varepsilon} \tag{2}$$

and $\varepsilon = (1 + 2\frac{\nu^2}{Q^2}\tan^2(\theta^2/2))^{-1}$ is the virtual photon polarization factor. One can then define the

beam spin asymmetry as follows.

$$BSA = \frac{d\sigma^+ - d\sigma^-}{d\sigma^+ + d\sigma^-} = \frac{\alpha \sin\phi_h}{1 + \beta\cos\phi_h + \gamma\cos(2\phi_h)} \tag{3}$$

Where several constants have been defined.

$$\alpha = \frac{\sqrt{2\varepsilon_L(1-\varepsilon)}}{\sigma_T + \varepsilon_L\sigma_L}\sigma_{LT'} \tag{4}$$

$$\beta = \frac{\sqrt{2\varepsilon_L(1+\varepsilon)}}{\sigma_T + \varepsilon_L\sigma_L}\sigma_{LT} \tag{5}$$

$$\gamma = \frac{\varepsilon}{\sigma_T + \varepsilon_L\sigma_L}\sigma_{TT} \tag{6}$$

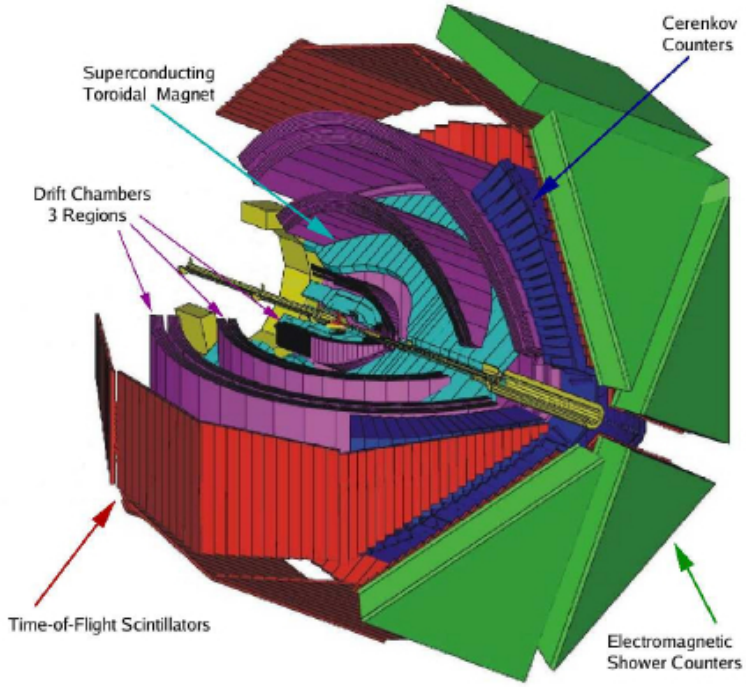


Figure 1: CLAS Detector shown with sub-systems labeled.

## 2 Experiment

This measurement was conducted at Jefferson Lab in Newport News, Virginia. Jefferson Lab houses the Continuous Electron Beam Accelerator Facility (CEBAF), as well as 4 experimental halls. The data used for this study was taken with the CEBAF Large Acceptance Spectrometer (CLAS) in Hall-B during 6 GeV operation.

The CLAS detector is composed of several sub-systems that are used together to infer the four momenta of particles that scatter out of the target. A central magnet provides a toroidal magnetic field used to separate charged particles and measure momentum, and divides the spectrometer azimuthally (in the x-y plane if z is taken to be the direction of the beam) into 6 identically constructed sectors. Each sector contains 4 major sub-systems:

- Drift Chambers - Used to detect tracks from charged particles and measure the particle momentum. Also responsible for most of the trajectory tracking of the particles.
- Cherenkov Counter - Used to separate electrons from negative hadrons.
- Electromagnetic Calorimeter - Records the energy deposited by charged and neutral particles, resposible for tracking photons/neutrons.

- Time of Flight Scintillators - A high resolution timing system that is used to calculate the velocity of particles. The time of flight system is the primary means used to separate different hadrons.

For the E1-F experimental run the beam energy was 5.5 GeV. The beam polarization was monitored with a Moller polarimeter, and the average value was found to be $\lambda_e = (75 \pm 3)\%$. The electron beam was incident on a liquid hydrogen target, 5 centimeters in length.

## 2.1 Electron Identification

Electrons are selected for analysis from the candidate tracks by using a cuts based classification algorithm. The dominant background for electron candidates are negative pions. All negative tracks are considered as possible electrons. These candidate electrons are first subject to geometric cuts.

As particles traverse the EC they create an electromagnetic shower, which is not confined within the detector when the particles pass close to the extremes of the detector strips. This mechanism leads to an underestimation of particle energy in the reconstruction phase, for that reason these tracks are discarded. Similarly, the detector efficiency is poorly understood at the extreme edges of the drift chambers, and tracks through these areas are also rejected.

The fractional energy deposition with respect to the particle momentum $E_{dep}/p$ is nearly constant as a function of momentum for electrons, but inversely depends on the momentum for negative pions. This property is exploited by placing a momentum dependent cut on the ratio $E_{dep}(p)/p$ for all negative candidate tracks. The ratio $E_{dep}/p$ is calculated in 60 momentum bins from 0.5 to 2.5 GeV/c (this should be double-checked). The electron signal is then fit with a Gaussian function, and the mean $\mu_i$ and standard deviations $\sigma_i$ are recorded for each momentum bin (above labeled i). These distributions are then fit with a 3rd order polynomial ($\mu(p) = ap^3 + bp^2 + cp + d$) and can be used to create decision boundaries for rejecting tracks from the candidate electron sample.

Unlike electrons, negative pions do not deposit a significant amount of energy in the inner EC, and we apply a minimum energy deposition cut to electron candidates ($E_{inner} > 50MeV$). The Cherenkov Counter (CC) is filled with $C_4F_{10}$ gas (perfluorobutane), which has a pion threshold of $p_\pi \approx 2.5GeV/c$. Historically, a cut was placed on the minimum number of photo-electrons detected for a track. This cut achieves the desired separation between electrions and negative pions, but is known to discard good electron candidates as well. For this analysis, we use a matching condition developed by Osipenko. Using the closest detector (drift chamber region 3) the track polar angle is calculated at the CC. This angle is compared with the CC detection segment for each of the 18 segments which span the polar angle up

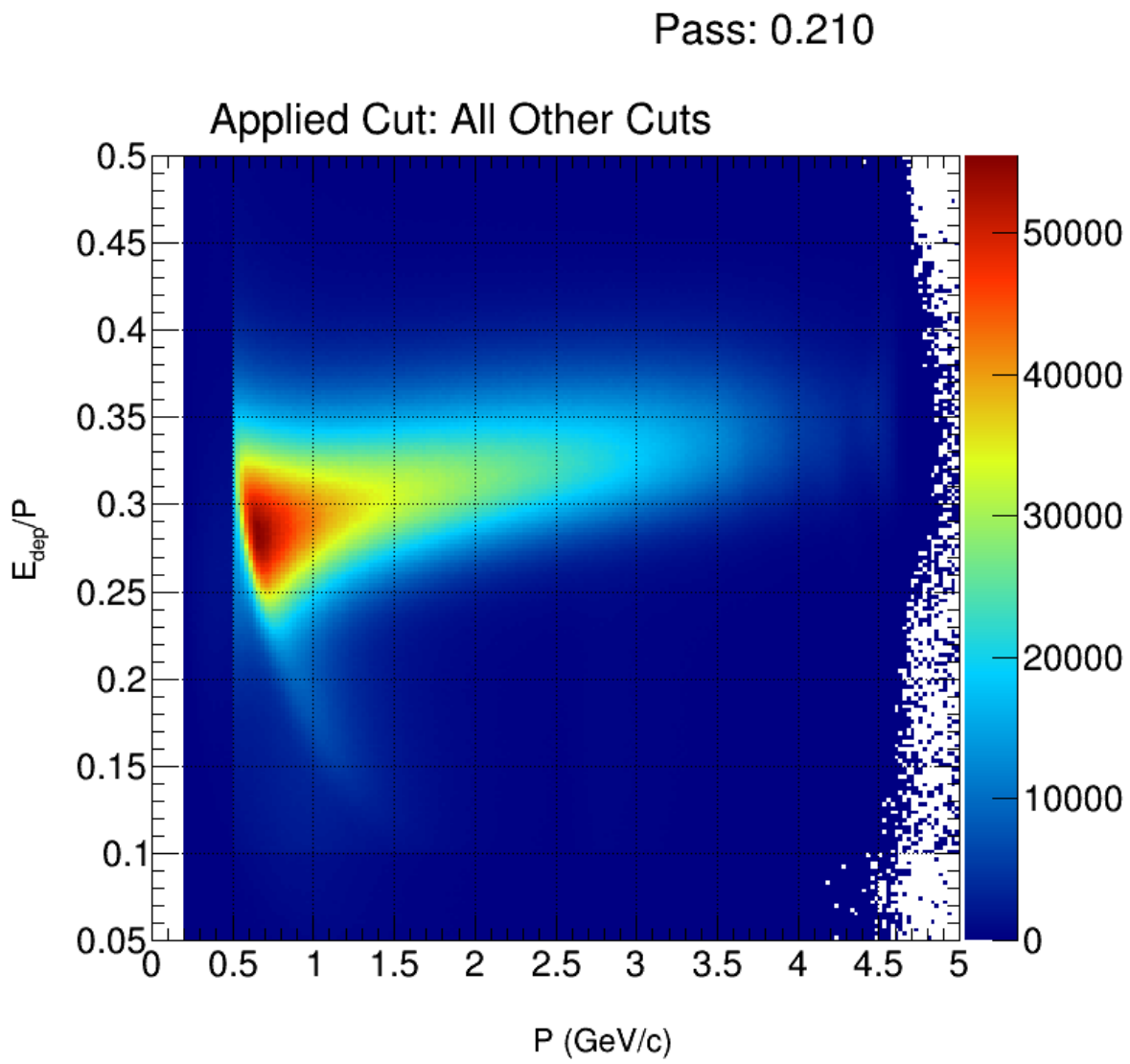


Figure 2: Sampling fraction for electron candidates (all other cuts passed).

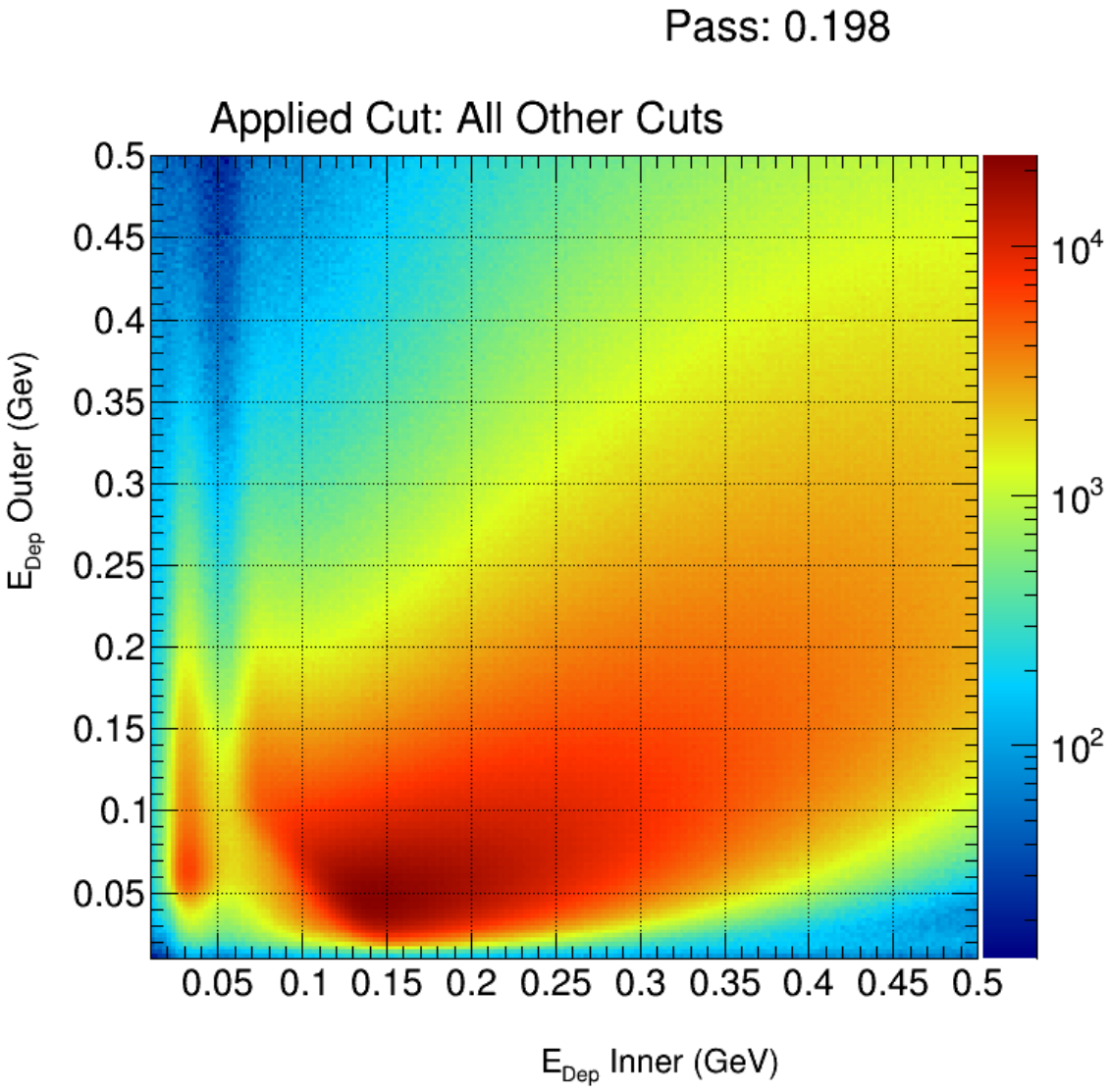


Figure 3: Calorimeter energy deposition for electron candidates (all other cuts passed).

to $\theta = 45°$. The procedure described above for fitting the momentum dependence of the ratio $E_{dep}/p$ is applied to the segment dependence of the angle $\theta_{CC}$.

## 2.2 Positive Pion Identification

After electron identification, all positive tracks are subject to two constraints. First, events which pass close to the torus coils are removed by cutting on the hit positions reported by the region 1 drift chambers, this is shown in figure 2.2. Such events are often poorly reconstructed or have poorly understood acceptances and are discarded from analyses. Then, the distance between the electron vertex and the positive track vertex is computed ($\delta v_z = v_z^e - v_z^+$). This distance is constrained to be within the length of the target (5 cm) see figure 2.2.

### 2.2.1 Likelihood Method

For each particle species considered, a normalized probability density function $P(x; p, h)$ is constructed for each input into the likelihood analysis. Here, x corresponds to the feature being used to catagorize different particles (in our case, x is the $\beta$ value measured by CLAS time-of-flight), p is the particle momentum, and h is the hadron being hypothesized (eg: in our case the possible values for h are pion, kaon, proton). In general if one uses a set of $N$ variables $x = (x_1, x_2, ..., x_N)$, the likelihood for a hypothesis h is defined below.

$$\mathcal{L}_h = \prod_{i=1}^{N} P_i(x_i; p, h) \tag{7}$$

In our case, the only random variable we consider is $\beta$, and the likelihood is just the PDF. Here, and in many cases where the choice is statistically appropriate, it is possible to use a Gaussian PDF for the variable $x_i$ ($\beta$).

$$P(\beta; p, h) = \frac{1}{\sqrt{2\pi}\sigma_\beta(p,h)} exp\left\{-\frac{1}{2}\left(\frac{\beta - \mu_\beta(p,h)}{\sigma_\beta(p,h)}\right)^2\right\} \tag{8}$$

The identity is assigned by choosing the particle hypothesis h which maximizes the likelihood ratio.

$$\frac{\mathcal{L}_h}{\mathcal{L}_\pi + \mathcal{L}_K + \mathcal{L}_p} \tag{9}$$

Using this method, every positive track is assigned a particle identification. However, at times the likelihood value is quite small when compared with the maximum likelihood for that species. This is the case for positrons which are classified by this method as positive pions, because they are the closest particle for which a hypothesis has been provided. To avoid these situations, the significance level $\alpha$ of

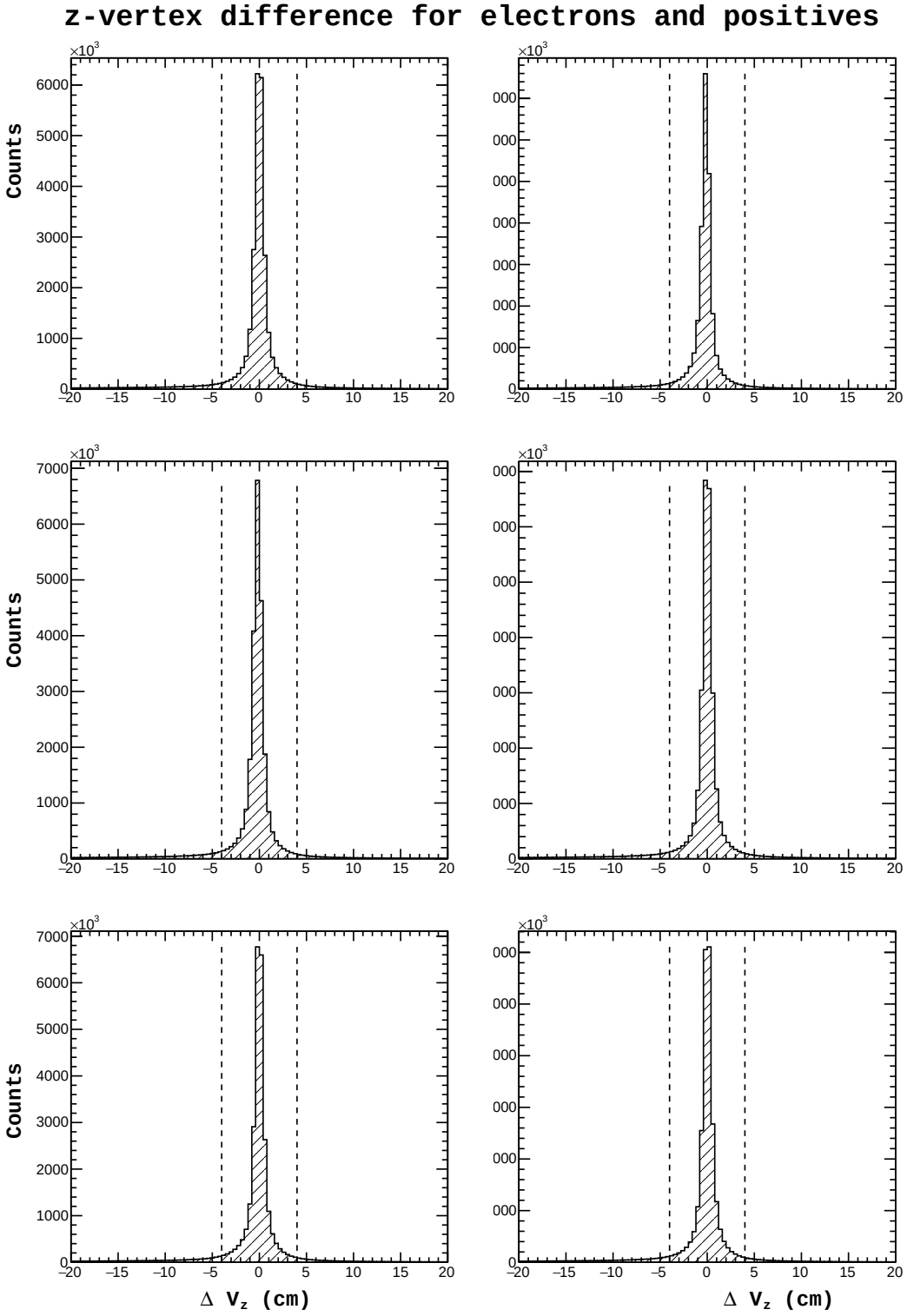


Figure 4: Shown above: The difference between the z-vertex position between detected electrons and positive tracks.

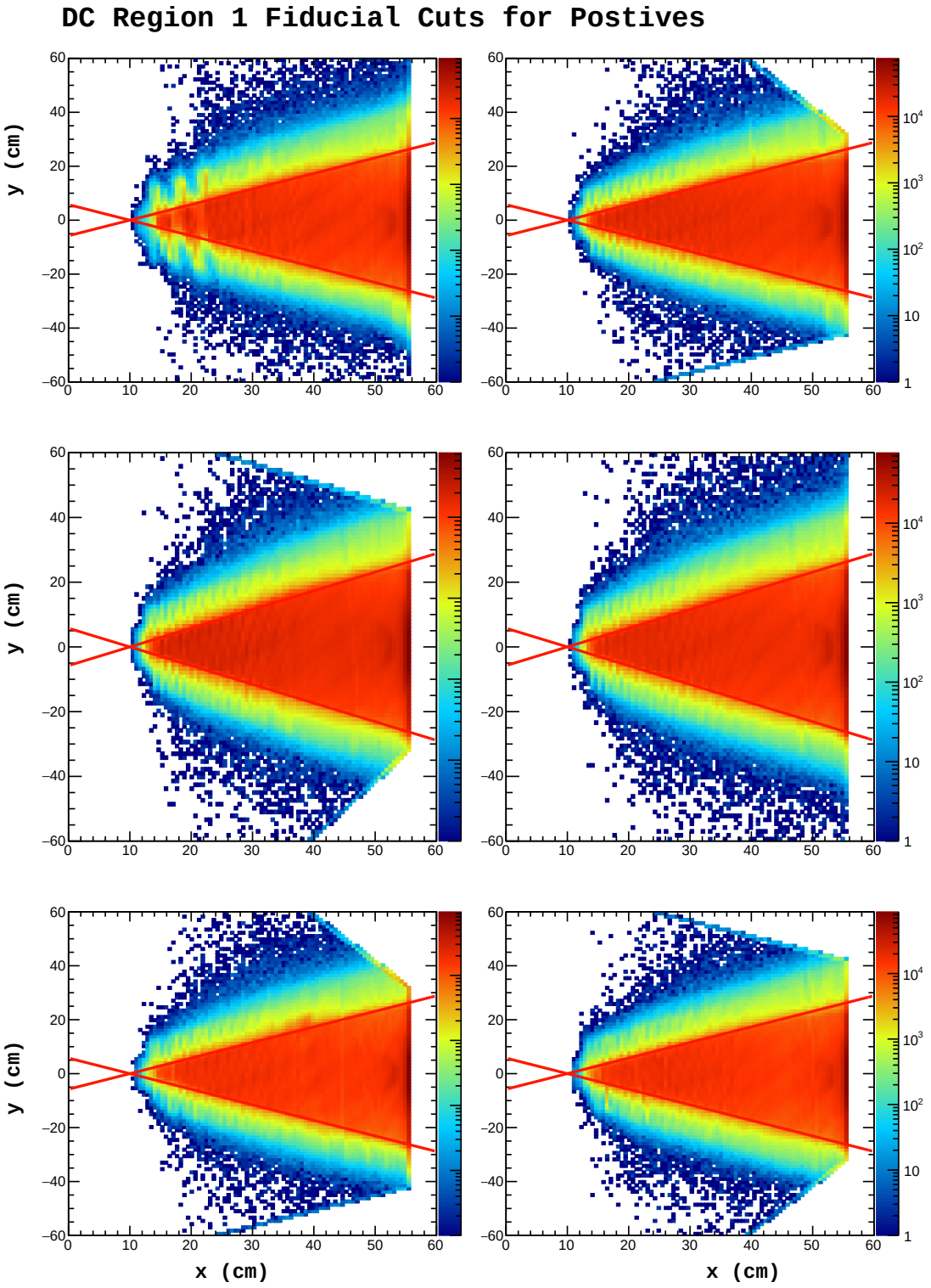


Figure 5: Shown above: Positive track hits on the region 1 drift chamber, events falling between the red lines are kept for analysis.

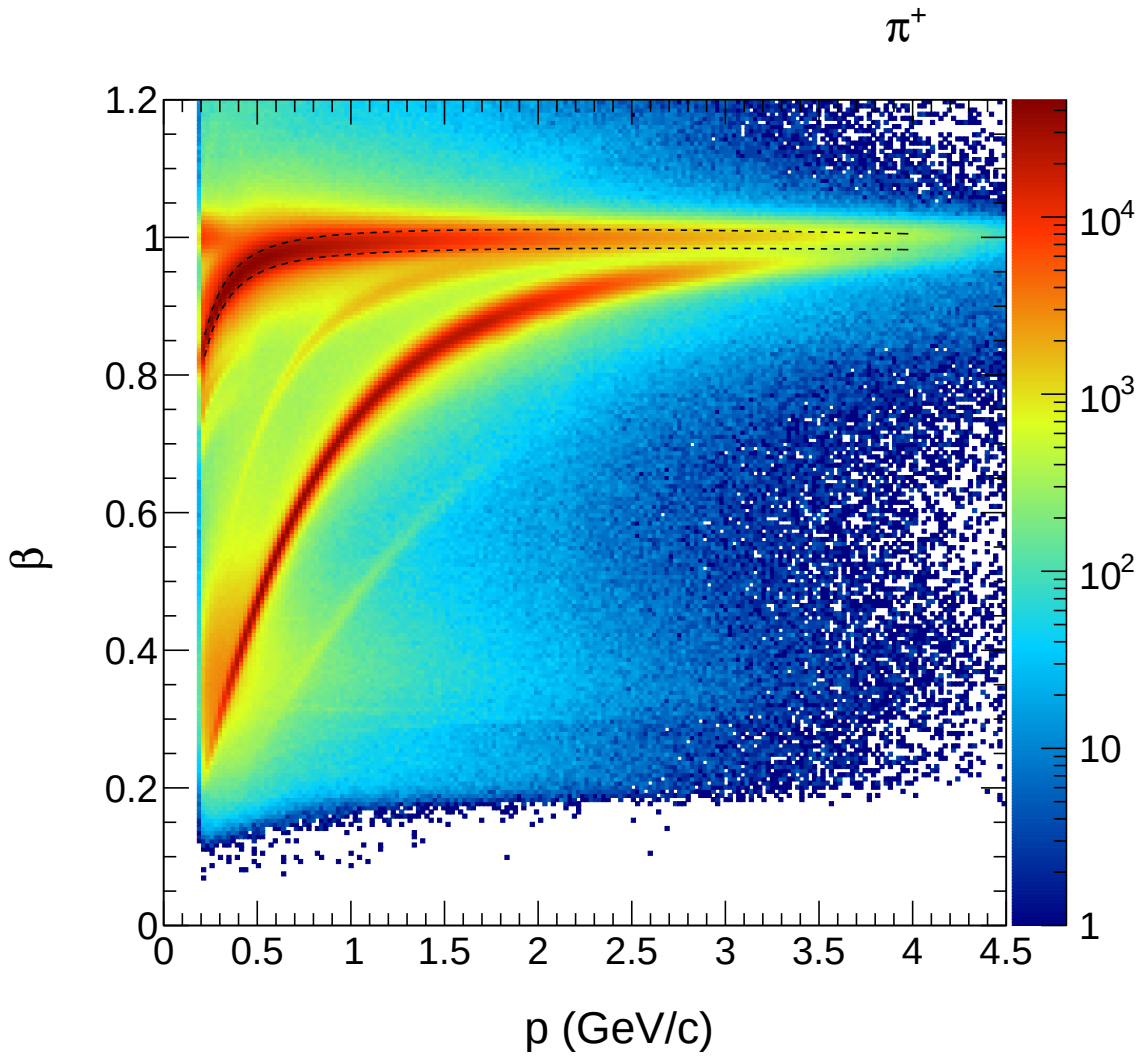


Figure 6: $\beta(p)$ resolution for positive pions shown.

each track is calculated and a cut is placed on the minumum significance. This cut can be easily varied to see how it changes the analysis result.

$$\alpha = 1 - \int_{\mu-\beta_{obs}}^{\mu+\beta_{obs}} P(\beta; p, h) d\beta \tag{10}$$

Pions are chosen using this method and we apply a cut on $\alpha > 0.05$.

# 3 Data Analysis

## 3.1 Corrections, Event Selection, & Binning

For this analysis $ep \to e\pi^+N$ events are identified by directly identifying the scattered electron and positive pion, and inferring the presence of the neutron.

After the electron and pion have been identified, their momenta are corrected using momentum corrections developed for the E1-F dataset by Marco Mirazita [3]. Time of flight corrections are also implemented based on work by Nathan Harrison [2], including removal of non-functional TOF paddles on a run-by-run basis.

After the particle identification and kinematic correction, kinematic restrictions of $Q^2 > 1.0$ and $W > 2.0$ are implemented to confine our measurement to the commonly accepted DIS region. The rest of the final state can be calculated for each event simply by comparing initial and final state four-vectors.

$$X^\mu = e'(k'^\mu) + \pi^+(h^\mu) - e(k^\mu) - p(P^\mu) \tag{11}$$

The missing neutron can be inferred by asking that $M_X = \sqrt{X^\mu X_\mu} \approx M_N$, in particular it is required that $0.89 < M_X < 1.01$. Events passing these criteria are considered to be the final event sample.

These events are binned in 15 bins (in the variable $\cos\theta_h$, the cosine of the polar angle between the virtual photon and the hadron) of variable size which are chosen based on the statistical content in each bin, and the acceptance in that bin. The most extreme backward angle was not used due to a large acceptance hole in the central phi regions, shown in figure (put figure and reference). The $\phi_h$ distributions are binned for fitting in 12 symmetric bins of width 30 degrees. (Add figure which shows the binning drawn over the phi vs. theta histogram).

## 3.2 Beam Spin Asymmetry

Beam spin asymmetry (BSA) measurements are a go-to tool for Nuclear/Particle Physics, and will now be briefly introduced. The cross section difference $d\sigma_+ - d\sigma_-$, where the subscript refers to the lepton (electron) helicity projection along the beamline direction, is just the part of the cross section which depends on the electron spin state. This quantity (interesting in itself) is not usually measured. Instead the ratio,

$$BSA = \frac{1}{P_e}\frac{d\sigma_+ - d\sigma_-}{d\sigma_+ + d\sigma_-} \approx \frac{1}{P_e}\frac{N_+ - N_-}{N_+ + N_-} \tag{12}$$

is presented, due to convenient cancellations in detector efficiency and acceptances in each cross section term. Where the fractional polarization of the beam is denoted as $P_e$. As mentioned in section 2, the beam spin is flipped at a rate of 33 Hz to minimize systematic errors arising due to differences in detector position and calibration.

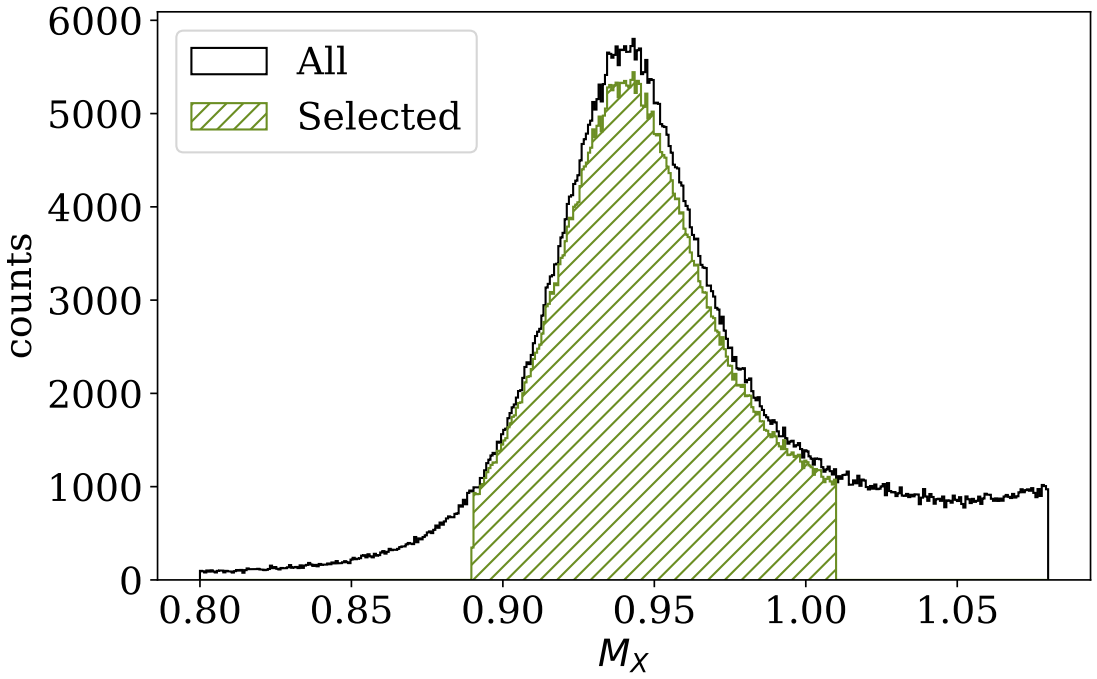


Figure 7: Missing mass cut used to select neutrons.

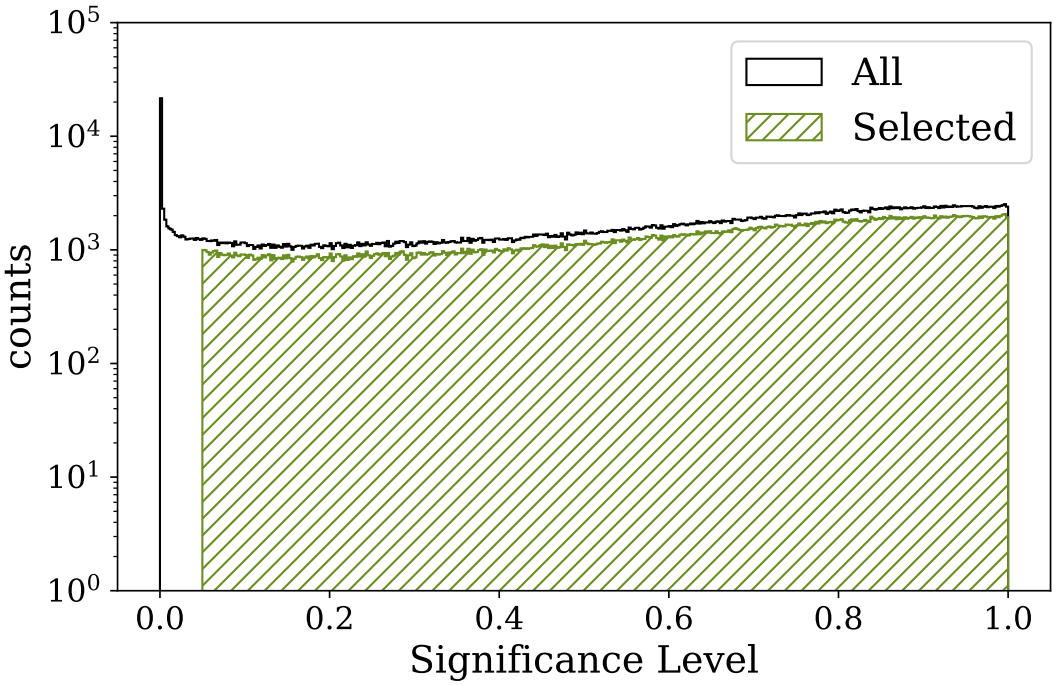


Figure 8: Significance level $\alpha$ before/after selection of final event sample.

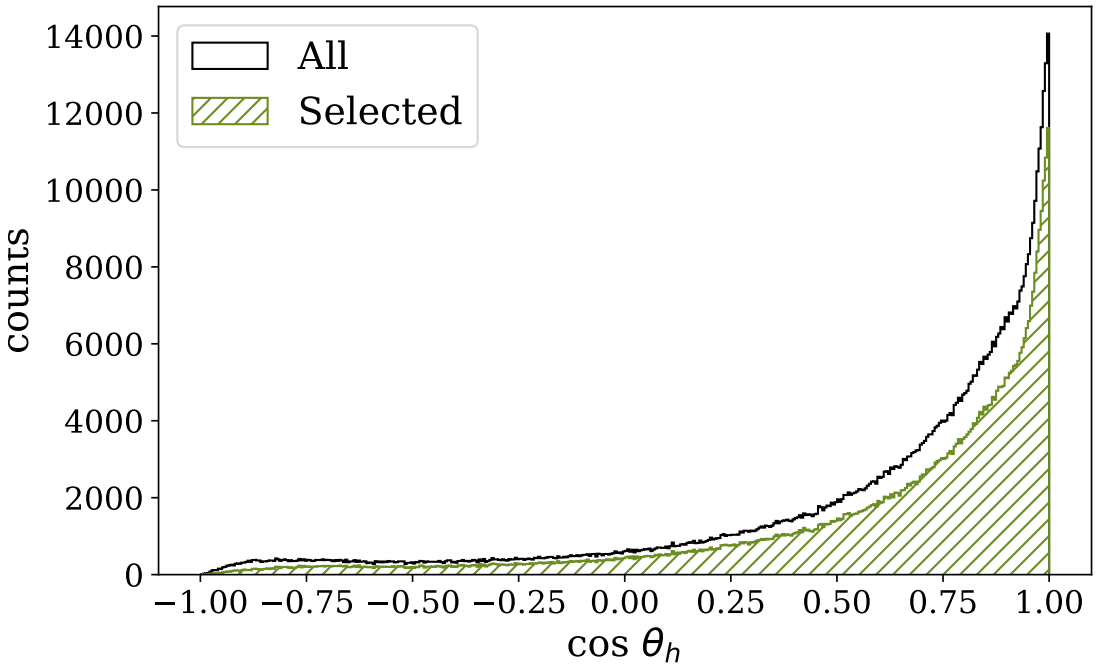


Figure 9: Distribution of $cos\theta_h$ for positive pions before and after missing mass and pion siginificance cuts.

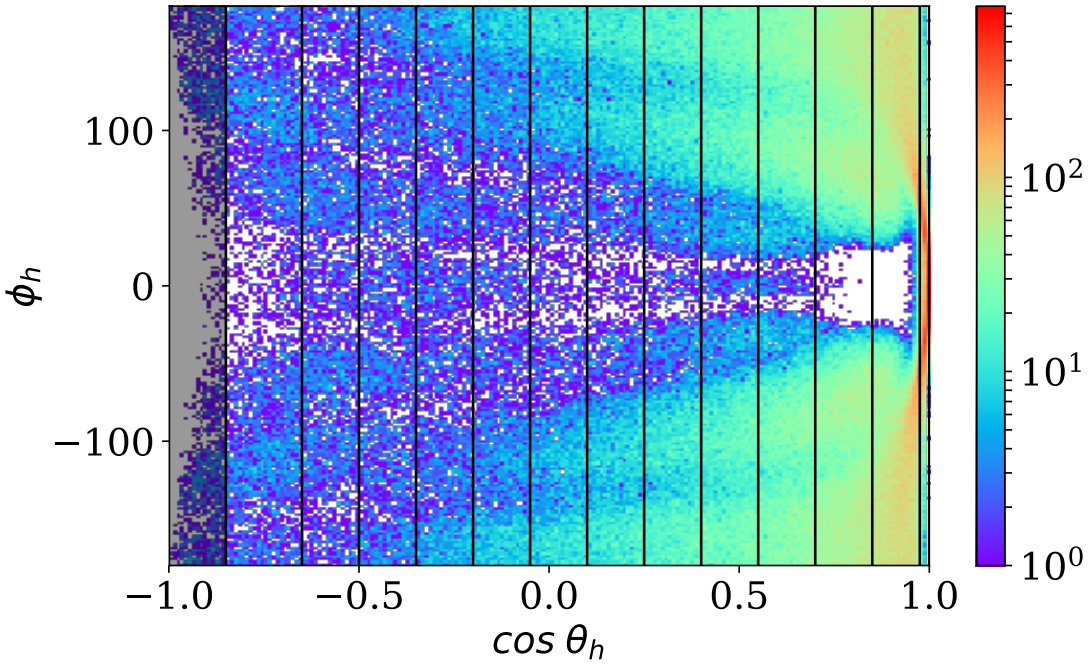


Figure 10: Distribution of events in the center of mass of the $\gamma^* p^+$ system. The extreme backward angles are removed for lack of data at central values of $\phi_h$.

## 3.3 Fitting Procedure

The distributions for $\phi_h$ are binned and fit with the function $f(\phi_h) = A \sin \phi_h$ using $\chi^2$ minimization. This is accomplished using the python implementation of gradient descent provided in `scipy.optimize.minimize`, which by default uses the `BFGS` method. Parameter errors are calculated using two methods, first the common Hessian method, and second the bootstrap replica method. These two methods are found to be consistent, and the parameter errors obtained by bootstrap methods are used throughout this report.

## 3.4 Systematic Errors

The error on our measured values is considered in two categories. First, statistical errors are calculated for the beam spin asymmetry measurement for every phi-bin. During the fitting procedure, these statistical errors are mapped into errors on the fit parameters. This first class of errors we consider as the statistcal error on the result. Second, the authors consider all other possible sources of error which do not depend on statistical effects. Those effects which have been identified are:

| Source | Relative Error |
|---|---|
| Cut: z-vertex | 0.0019 |
| Cut: `EC edep` | 0.0027 |
| Cut: sampling fraction | 0.0010 |
| Cut: $\theta_{CC}$ matching | 0.0022 |
| Cut: pion significance $\alpha$ | 0.0049 |
| Beam Polarization | 0.03 |

### 3.4.1 Cut Variations

In some cases, the direct variation of analyses parameters is the only way to try and understand the dependence of the result on the input parameters. Ideally, the analysis result shouldn't vary outside of the errors which arise from statical fluctuations.

### 3.4.2 Random Subset/Helicity

Two additional studies are performed which involve randomization of the input data in some way. In the first study, the helicity of each event is assigned a random value of $\pm 1$. This randomization destroys the correlation between beam spin and the $\phi_h$ distributions. Therefore, one expects to find zero asymmetries as a result of this randomization. In the second study, the full analysis is run on a subset of 80% of

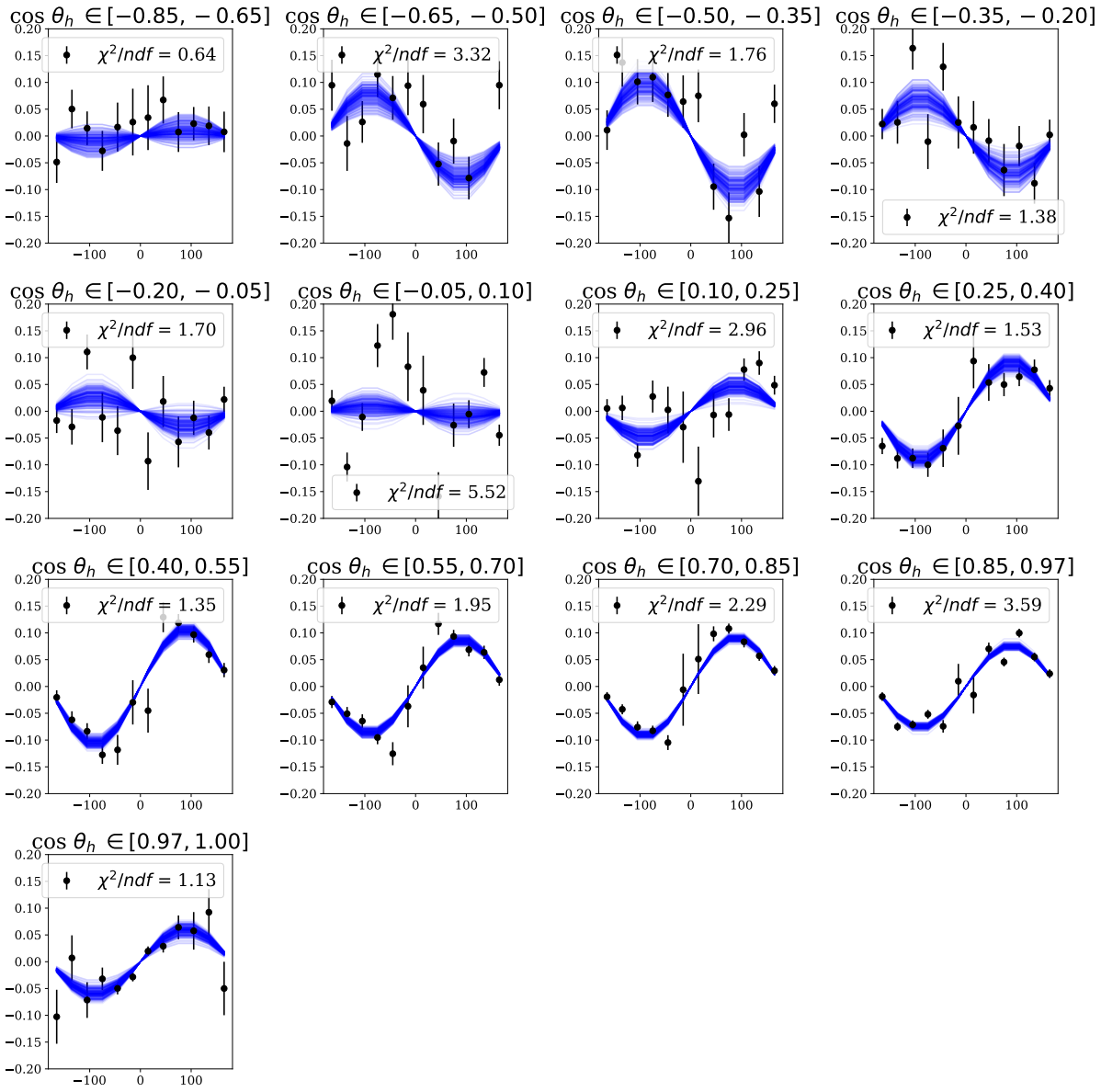


Figure 11: The BSA shown as a function of $\phi_h$ for different bins of $\cos\theta_h$. Overlaid are the 200 bootstraps performed for each $\cos\theta_h$-bin.

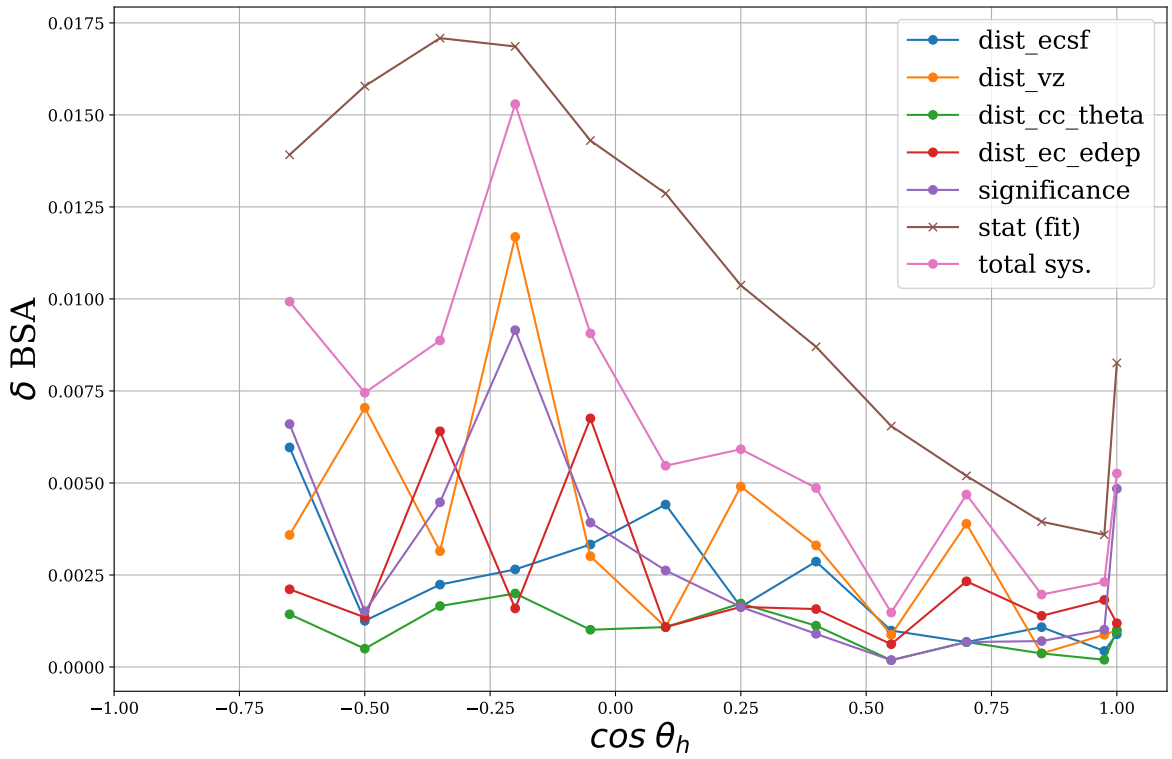


Figure 12: The largest shift resulting from all variations of each analysis cut parameter. Shown also is the statistical error. All resulting cut variations remained withtin statistical error.

the events in the full dataset. This study is designed to identify if there is internal inconsistancy in the dataset.

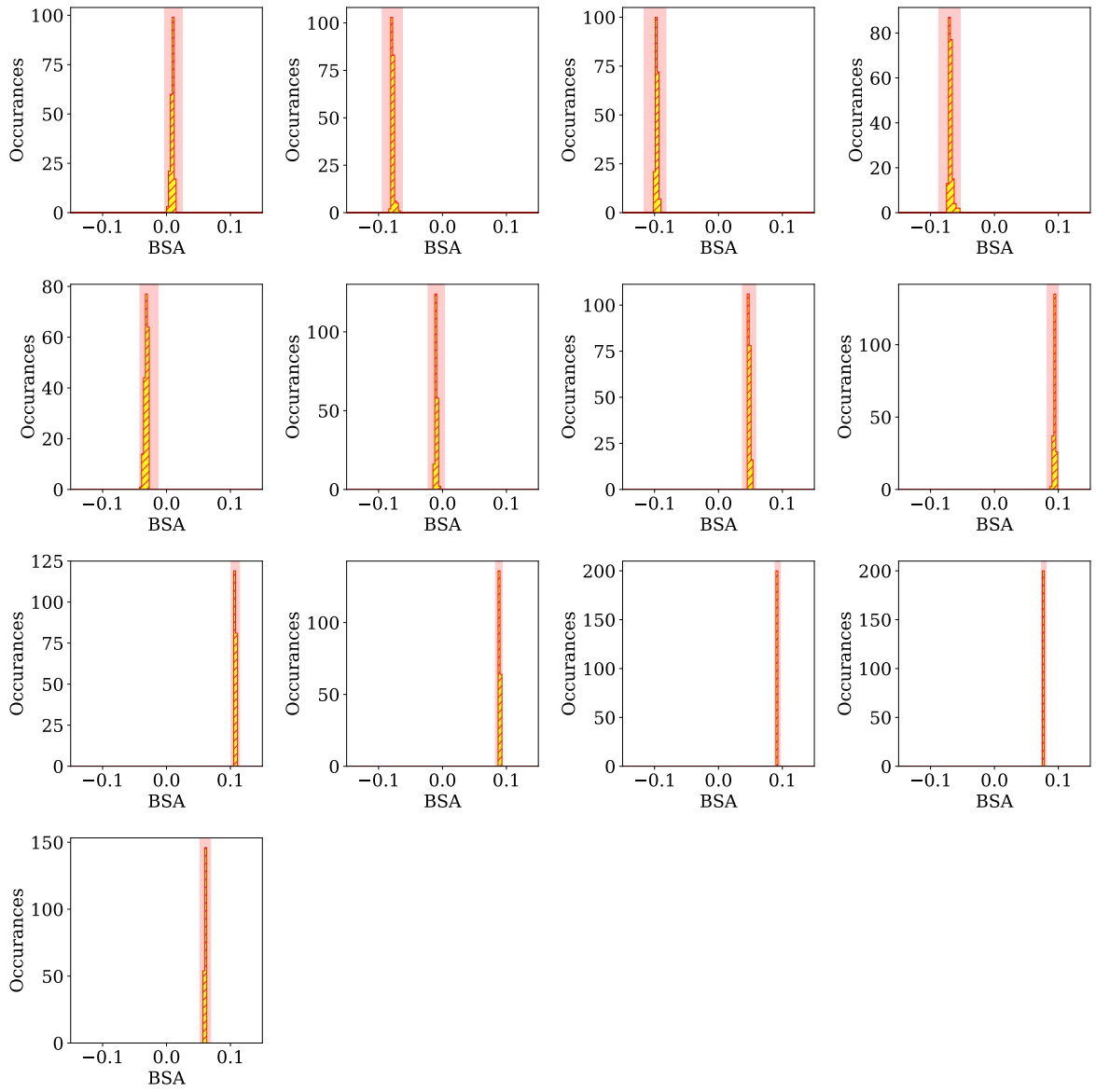


Figure 13: Results for each bin of $\cos(\theta_h)$ calculated on 200 random subsets of 80% of the entire dataset. In the absence of internal inconsistency in the data, these results should be gaussianly distributed around the nominal result obtained with the entire dataset, which is shown with statistical error in red.

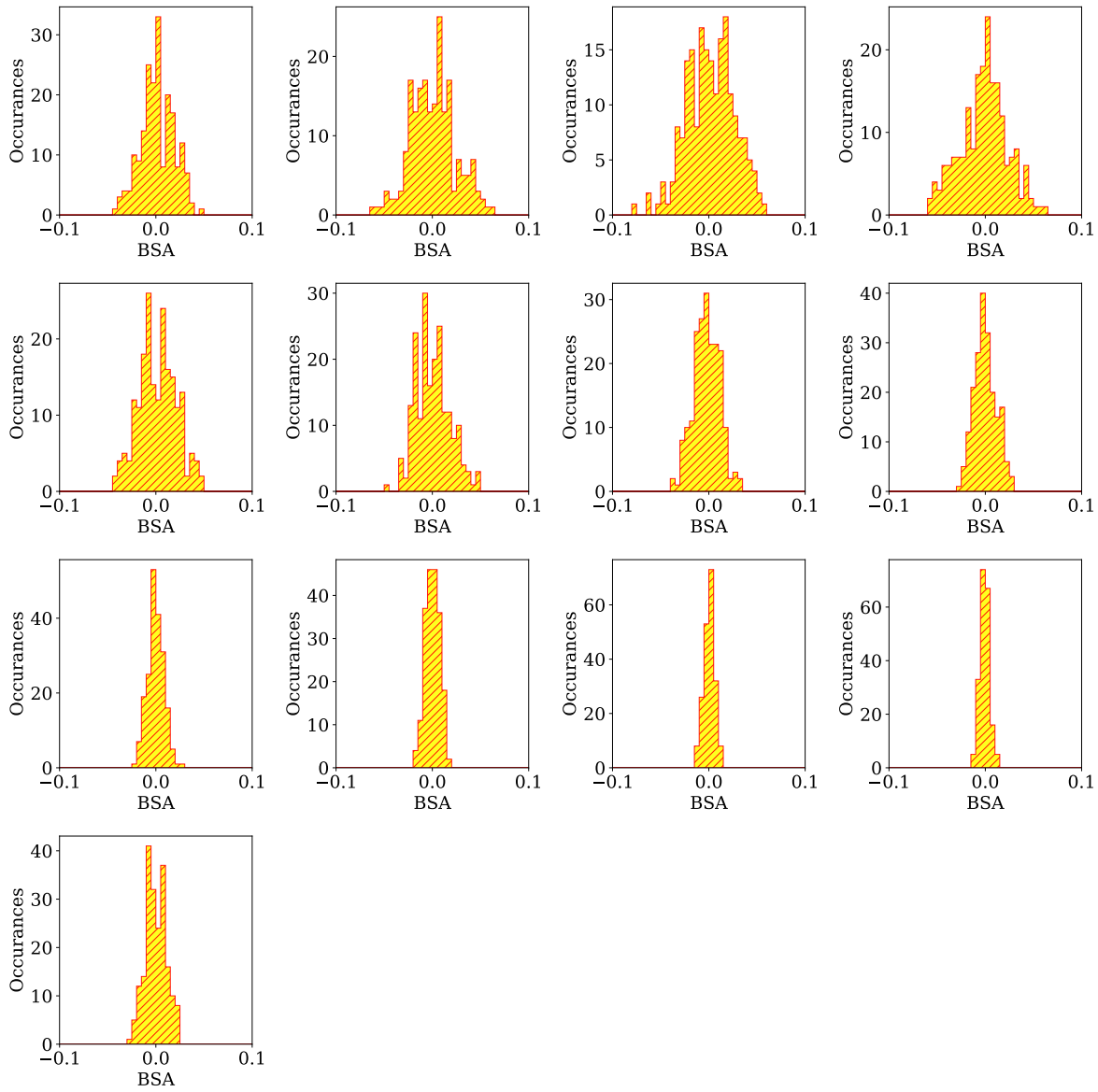


Figure 14: Shown above are the results for randomizing the helicty for every event, and repeating the analysis 200 times. This randomization destroys any correlation between the helicity states and the cross section, meaning that these results are expected to be zero (with larger fluctuation in lower statistics bins).

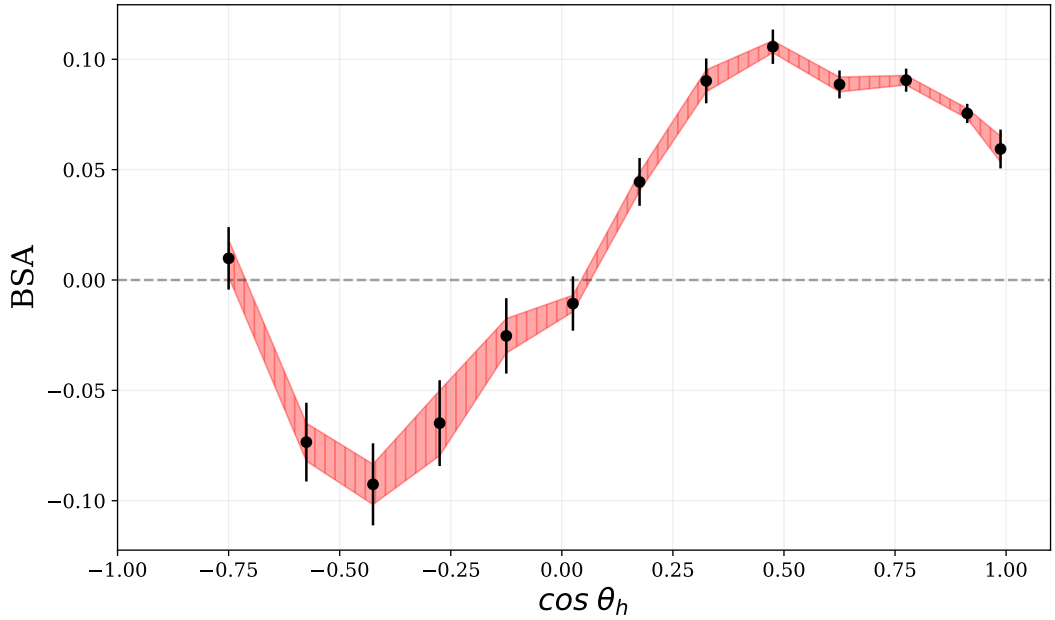


Figure 15: BSA shown with systematic errors in blue.

# 4 Results

This section will display the final results for the BSA. We will also compare to previously measured results, as well as compare to theory if any is available.

## 4.1 Comparison to Other Measurements

Here we are comparing to E1-6.

# References

[1] D. Drechsel and L. Tiator. "Threshold Pion Production on Nucleons". In: *J. Phys. G 18 449* (1992).

[2] Nathan Harrison. "Semi-Inclusive Pion Electronproduciton on the Proton". In: ().

[3] Marco Mirazita. "Momentum Corrections for E1-F". In: ().